Lawrence Berkeley National Laboratory
Recent Work

Title

CORROSION OF A ROTATING IRON DISK IN LAMINAR, TRANSITION, AND FULLY-DEVELOPED TURBULENT FLOW

Permalink

https://escholarship.org/uc/item/8957j3kj

Authors

Law, C.G.
Newman, J.

Publication Date

1984-07-01

eScholarship.org Powered by the California Digital Library
University of California

UC-25
LBL-18157
Preprint

Lawrence Berkeley Laboratory
UNIVERSITY OF CALIFORNIA

RECEIVED
LAWRENCE
BERKELEY LABORATORY
Sep 10 1984
LIBRARY AND
DOCUMENTS SECTION

Materials & Molecular Research Division

Submitted to the Journal of the Electrochemical Society

CORROSION OF A ROTATING IRON DISK IN LAMINAR, TRANSITION, AND FULLY-DEVELOPED TURBULENT FLOW

C.G. Law, Jr. and J. Newman

July 1984

For Reference
Not to be taken from this room

Prepared for the U.S. Department of Energy under Contract DE-AC03-76SF00098

LBL-18157

DISCLAIMER

This document was prepared as an account of work sponsored by the United States Government. While this document is believed to contain correct information, neither the United States Government nor any agency thereof, nor the Regents of the University of California, nor any of their employees, makes any warranty, express or implied, or assumes any legal responsibility for the accuracy, completeness, or usefulness of any information, apparatus, product, or process disclosed, or represents that its use would not infringe privately owned rights. Reference herein to any specific commercial product, process, or service by its trade name, trademark, manufacturer, or otherwise, does not necessarily constitute or imply its endorsement, recommendation, or favoring by the United States Government or any agency thereof, or the Regents of the University of California. The views and opinions of authors expressed herein do not necessarily state or reflect those of the United States Government or any agency thereof or the Regents of the University of California.

CORROSION OF A ROTATING IRON DISK IN LAMINAR, TRANSITION, AND FULLY-DEVELOPED TURBULENT FLOW

Clarence G. Law, Jr.* and John Newman

Materials and Molecular Research Division, Lawrence Berkeley Laboratory, and Department of Chemical Engineering, University of California, Berkeley, California 94720

July, 1984

Abstract

Electrochemical corrosion generally involves the interaction of numerous phenomena. A model is presented which accounts for the different hydrodynamic regimes across the surface, ohmic potential variations, and the simultaneous occurrence of oxygen reduction and the oxidation of iron. The active-passive transition for iron is presumed to occur at a specific value of the electrode potential. Results illustrate the importance of disk size, oxygen concentration, and solution conductivity upon the corrosion rate distribution. The calculations also compare well to the experimental results of LaQue.

Key words: passivation, mass transfer

*Present address: AT&T Technologies, Inc., P. O. Box 900, Princeton, NJ 08540.

INTRODUCTION

The rotating disk is an excellent system for the study of localized corrosion.[1] Much is known about fluid flow, mass transfer, and electrochemical kinetics on a rotating disk in laminar flow.[2,3] However, because the mass transport rate is uniform across the surface in laminar flow, a uniform corrosion rate may occur. Consequently, laminar flow results do not reveal much information concerning the interaction of ohmic drop, electrochemical kinetics, and mass transfer to determine overall corrosion rates and their distribution. When transition and fully-developed turbulent flow exist on the surface, the nonuniform mass-transfer rate results in a nonuniform heterogeneous reaction rate distribution. In earlier work,[4] the mass-transfer rates in transition and turbulent flow were calculated. These results can be used here to calculate the corrosion rates for a disk upon which the three different flow regimes may exist simultaneously.

Some time ago, LaQue[5] reported the results of corrosion experiments with rotating disks in sea water. The interesting feature of the results is the difference in behavior between iron and copper disks. For copper disks, the most severe corrosion attack occurred near the periphery. The central region remained almost unattacked. However, the iron disks were corroded near the center and not near the edge. In photographs of iron disks given by LaQue, one can see the clear demarcation between the attacked region in the center and the low corrosion region near the edge.

LaQue used iron disks of 3, 4, and 5 inches in diameter rotated at 122/s in sea water. The Reynolds number is sufficiently large for the periphery to be in fully-developed turbulent flow. With the benefit of the mass-transfer

rates for large Reynolds numbers and a kinetic expression for a sharp demarcation between active and passive states, a model is developed which allows comparison with LaQue's data. This is an improvement over the work by Vahdat and Newman,[6] which permitted qualitative comparison with the experimental evidence. The present approach is aimed at removing some of these limitations to show quantitative agreement with the experimental data.

Model Development

The corrosion reactions on the surface can be expressed as:

$$Fe \rightarrow Fe^{++} + 2e^{-} \tag{1}$$

$$O_2 + 2H_2O + 4e^{-} \rightarrow 4OH^{-} \tag{2}$$

The rate of each reaction varies across the surface. For corrosion to occur, the total current from the anodic reaction must balance the total from the cathodic reaction, hence

$$I = 0 = I_{Fe^{++}} + I_{O_2} \tag{3}$$

A model must consider the kinetic rates of the two reactions, the potential variation across the surface, and the mass-transfer rate through the diffusion layer.

Electrochemical Kinetics

Since iron is an active-passive metal, the form of the electrochemical reaction is dependent upon the potential range under consideration. For values of $(V-\Phi_0) \leq (V-\Phi_0)_*$, the reaction is considered active. However, for larger values of the driving force, a passive film is presumed to exist. The presence of this film prevents significant electrochemical reaction. From Pourbaix's results,[7] it is possible to obtain the current density at $(V-\Phi_0)_*$, where $(V-\Phi_0)_*$ is the value of the potential corresponding to the maximum current possible.

Corrosion of an iron rotating disk in an oxygenated salt solution is an example of the occurrence of simultaneous electrochemical reactions. An individual reaction can be written in general form

$$\sum_i s_{ij} M_i^{z_i} \rightarrow n_j e^- \quad , \tag{4}$$

where n_j is the number of electrons transferred, s_{ij} is the stoichiometric coefficient for species i in reaction j, and M_i represents chemical species i with charge z_i. The local rate of each individual reaction is given by i_j and is related to the total rate by

$$i_T = \sum_j i_j \quad . \tag{5}$$

The flux of an individual species at the surface is related to its participation in each reaction by

$$N_i(r) = - \sum_j \frac{s_{ij}\, i_j}{n_j F} \quad . \tag{6}$$

A Butler-Volmer expression can be used to express the local current density of each reaction i_j in terms of the local value of the surface overpotential

$$i_j = i_{0,j} \left[e^{\frac{\alpha_a F}{RT} \eta_s} - e^{\frac{-\alpha_c F}{RT} \eta_s} \right] \quad . \tag{7}$$

The exchange current density can be written as

$$i_{0,j} = i_{0,j\mathrm{ref}} \prod_i \left(\frac{c_{i,0}}{c_{i,\mathrm{ref}}} \right)^{\gamma_{ij}} \quad , \tag{8}$$

and

$$\gamma_{ij} = q_{ij} + \frac{\alpha_{cj} s_{ij}}{n_j} \quad , \tag{9}$$

where $q_{ij} = -s_{ij}$ for a cathodic reactant and zero otherwise. The surface

overpotential is defined by

$$\eta_s = V - \Phi_0 - U_{j,0} \quad . \tag{10}$$

V is the potential of the iron disk; Φ_0 is the potential in the solution just outside the double layer; and $U_{j,0}$ is the theoretical open circuit cell potential for reaction j. $U_{j,0}$ is expressed as

$$U_{j,0} = U_j^\theta - U_{ref}^\theta - \frac{RT}{n_j F} \sum_i s_{ij} \ell n \left(\frac{c_{i,0}}{\rho_0}\right) + \frac{RT}{n_{ref} F} \sum_i s_{i,ref} \ell n \left(\frac{c_{i,ref}}{\rho_0}\right) \tag{11}$$

provided that activity-coefficient corrections can be neglected. For the work given here, the saturated calomel electrode is chosen as the specific reference electrode. With the definitions given above, the expressions for the iron and oxygen current densities can be expressed as

$$i_{Fe^{++}} = \frac{i_{0Fe^{++},ref}}{\left(c_{Fe^{++},ref}/\rho_0\right)^{\alpha_a/n_{Fe^{++}}}} \exp\left[\frac{\alpha_a F}{RT}\left(V_M - U^\theta_{Fe^{++}}\right)\right] \left\{\exp\left[\frac{\alpha_a F}{RT}\left(V-\Phi_0\right)\right] - \left(\frac{c_{Fe^{++},0}}{\rho_0}\right) \exp\left[\left(\alpha_a+\alpha_c\right)\frac{F}{RT}\left(V_M - U^\theta_{Fe^{++}}\right)\right] \exp\left[\frac{-\alpha_c F}{RT}\left(V-\Phi_0\right)\right]\right\} \quad \text{and} \tag{12}$$

$$i_{O_2} = \frac{i_{0O_2,ref} \exp\left[\frac{-\alpha_a F}{RT}\left(V_M - U^\theta_{O_2}\right)\right]}{\left(c_{O_2,ref}/\rho_0\right)^{1-\alpha_c/n_{O_2}} \left(c_{OH,ref}/\rho_0\right)^{\alpha_c}} \left\{\left(\frac{c_{OH,0}}{\rho_0}\right)^{\alpha_c} \exp\left[\frac{\alpha_a F}{RT}\left(V-\Phi_0\right)\right] - \exp\left[\left(\alpha_a+\alpha_c\right)\frac{F}{RT}\left(V_M - U^\theta_{O_2}\right)\right] \left(\frac{c_{O_2}}{\rho_0}\right) \exp\left[\frac{-\alpha_c F}{RT}\left(V-\Phi_0\right)\right]\right\} , \tag{13}$$

where

$$V_M = U^\theta_{Hg_2Cl_2} + \frac{F}{RT} \ell n \left(c_{Cl,ref}\right) \quad . \tag{14}$$

This expression for the iron current density applies only to the active region where $V - \Phi_0 \leq (V-\Phi_0)_* = -0.4676$ V. For the passive region existing for larger values of $V - \Phi_0$, $i_{Fe^{++}} = i_p$. Although the transfer coefficients are not subscripted for the respective reactions, they are different for each. An illustration of the active-passive kinetic relationship is presented in figure 1. The parameters used for the iron and oxygen reaction are given in table I.

Potential Distribution

From previous work on rotating disk systems, the solution of Laplace's equation for the potential can be expressed as

$$\Phi(\eta,\xi) = \sum_{n=0}^{\infty} Q_n P_{2n}(\eta)\, M_{2n}(\xi) \tag{15}$$

where η and ξ are rotational elliptic coordinates. These are related to cylindrical coordinates by

$$y = r_0\, \xi\, \eta \tag{16}$$

$$r = r_0 \sqrt{(1 + \xi^2)(1 - \eta^2)} \tag{17}$$

$P_{2n}(\eta)$ is the Legendre polynomial of order 2n. $M_{2n}(\xi)$ is the Legendre function of imaginary argument defined to that $M_{2n} = 1$ at $\xi = 0$.

The diffusion layer is also considered thin enough so that the local current density can be obtained from the sum of the partial currents or from the potential derivative at the surface. An additional equality is added to equation 5 to give

$$i_T = \sum_j i_j = -\kappa_\infty \left.\frac{\partial \Phi}{\partial y}\right|_{y=0} \tag{18}$$

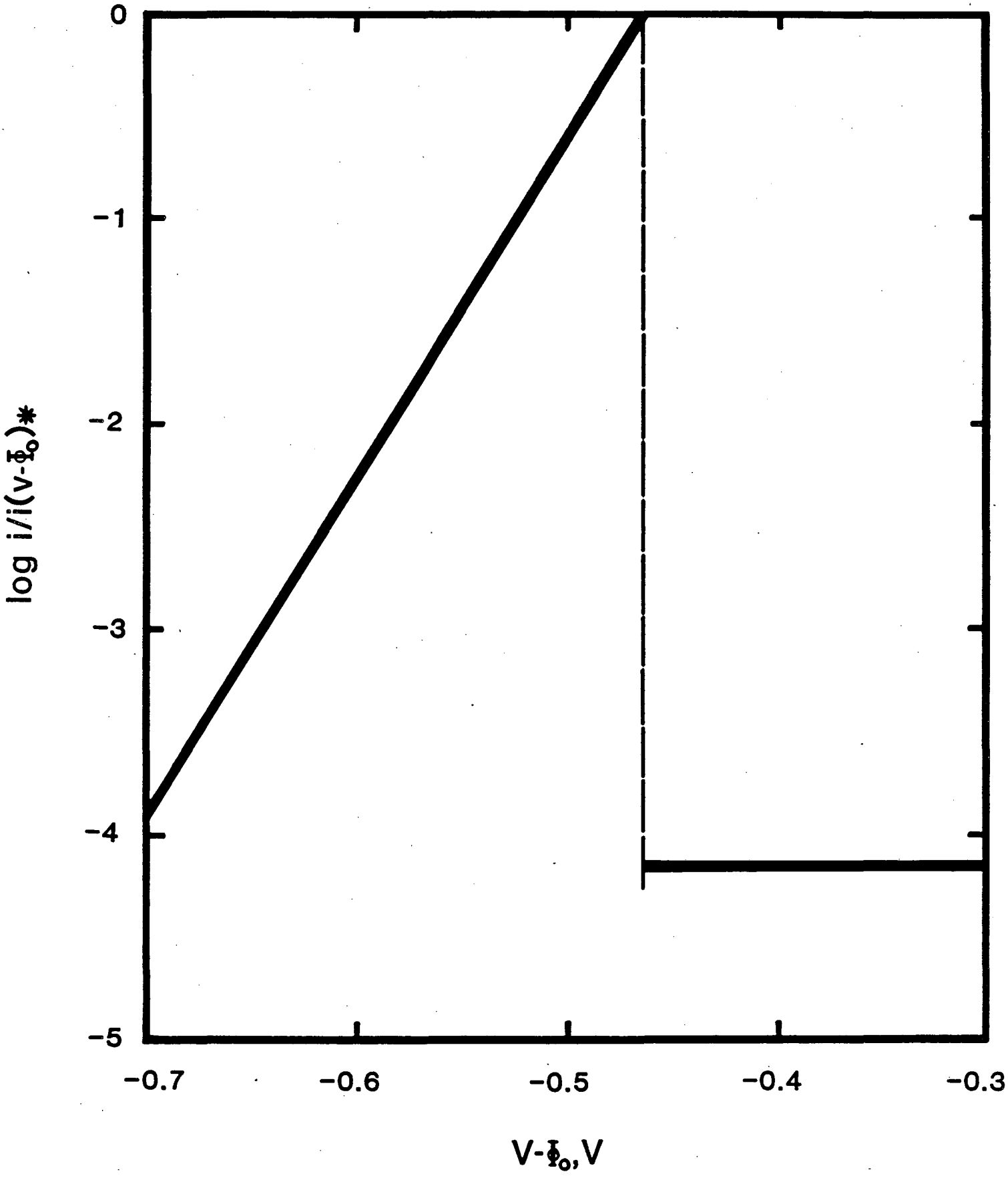

XBL 848-8614

Figure 1. Normalized iron current density vs. potential driving force

Table I

Kinetic Parameters

Iron	Oxygen
$\alpha_a = 1.0$	$\alpha_a = 3.0$
$\alpha_c = 1.0$	$\alpha_c = 1.0$
$n = 2.0$	$n = 4.0$
$i_{0Fe^{++},ref} = 1.098 \times 10^{-6}$ A/cm^2	$i_{0O_{2ref}} = 7.4 \times 10^{-4}$ A/cm^2
$c_{Fe^{++},ref} = 4.0$ moles/litre	$c_{O_{2ref}} = 1.0 \times 10^{-4}$ moles/litre
$c_{Fe^{++},0} = 5.3 \times 10^{-4}$ moles/litre	

$$i_{Fe^{++}\ (V-\Phi_0)_*} = 1.5 \times 10^{-3}\ \text{A/cm}^2$$

From the orthogonal properties of Legendre polynomials, the constants in the series solution for the potential distribution are given as

$$Q_n = \left[P_{2n}(0)\right]^2 \frac{(4n+1)\pi r_0}{2\kappa_\infty} \int_0^1 \eta\, i_T\, P_{2n}(\eta)\, d\eta \qquad (19)$$

To obtain the potential distribution when the iron current density can discontinuously change from the value given by equation 12 at $V - \Phi_0 = (V - \Phi_0)_*$ at position r_p to $i = i_p$, it is convenient to consider the potential associated with each reaction differently. From equation 18 we can write

$$i_T = (i_{Fe^{++}} - i_p) + (i_{O_2} + i_p) \qquad (20)$$

The potential distribution is

$$\Phi(\eta,\xi) = \sum_{n=0}^{\infty} B_n P_{2n}(\eta_p) M_{2n}(\xi_p) + \sum_{n=0}^{\infty} D_n P_{2n}(\eta) M_{2n}(\xi) \qquad (21)$$

where η_p and ξ_p are defined in equations 16 and 17 with r_0 replaced with r_p.

$$B_n = \left[P_{2n}(0)\right]^2 \frac{(4n+1)\pi r_p}{2\kappa_\infty} \int_0^1 \eta_p (i_{Fe^{++}} - i_p)\, P_{2n}(\eta_p)\, d\eta_p \qquad (22)$$

$$D_n = \left[P_{2n}(0)\right]^2 \frac{(4n+1)\pi r_0}{2\kappa_\infty} \int_0^1 \eta (i_{O_2} + i_p) P_{2n}(\eta)\, d\eta \qquad (23)$$

The potential on the surface of the disk is given by

$$\Phi_0(\eta, \xi = 0) = \sum_{n=0}^{\infty} B_n P_{2n}(\eta_p) M_{2n}(\xi_p) + \sum_{n=0}^{\infty} D_n P_{2n}(\eta) \qquad (24)$$

Diffusion Layer

The mass-transfer rate of species to the surface must be in harmony with electrochemical kinetics and the ohmic potential distribution across the surface. With an excess of supporting electrolyte, the mass flux of minor species at the surface can be expressed in terms of a superposition integral. A result of the work of Smyrl and Newman[8] expressed in terms of the variables of this problem is

$$\left.\frac{\partial c_i}{\partial y}\right|_{y=0} = \frac{-\sqrt{r\beta}}{\Gamma(4/3)} \int_o^x \left.\frac{dc_o}{dx}\right|_{x=x_o} \frac{dx_o}{\left[9D_i \int_{x_o}^{x} r\sqrt{r\beta}\, dx\right]^{1/3}} \quad . \tag{25}$$

Although this relationship is true for laminar, transition, or fully-developed turbulent flow, the specific details vary. In particular, the level of turbulence varies as does the shear stress.

In earlier work,[4] results were given for the mass-transfer rate to rotating rings and rotating disks when laminar, transition, and fully-developed turbulent flow exist simultaneously on the surface. These theoretical and experimental results apply to the mass-transfer limiting case.

For the corrosion problem of interest here, the concentration can be expressed as an integral of the previously obtained mass-transfer results given by

$$c_i(z,\zeta) = c_{i,\infty} + \int_0^z \left.\frac{dc_{i,0}}{dz}\right|_{z=z'} \left[1 - \theta(z,z';\zeta)\right] dz' \quad , \tag{26}$$

where

$$z = 9K \int_0^R R\sqrt{R\,\beta/\Omega}\, dR \quad , \tag{27}$$

$$R = r\sqrt{\Omega/\nu} = \sqrt{Re} \quad , \tag{28}$$

K is a constant in the correlation of the eddy diffusivity,

ζ is the Lighthill variable which can be expressed as

$$\zeta = \left(\frac{\Omega^{1/2} K^{1/3}}{\nu^{1/6} D_i^{1/3}} \right) \frac{\sqrt{R \beta/\Omega}\, y}{(z-z')^{1/3}} \quad , \tag{29}$$

$\theta(z,z',\zeta)$ represents the concentration at position (z,ζ) when the mass transfer begins at position (z',ζ). $\theta(z,z',\zeta = 0)$ is zero for $z \geq z'$, otherwise it is 1.

For the reader interested in more detail, the development of the fundamental solution, $\theta(z, z',\zeta)$ is presented.

When laminar, transition, and full-developed turbulent flow exist on the surface, the radial shear stress must vary to reflect the different hydrodynamic conditions. The laminar flow form is well known; the fully-developed turbulent flow form is consistent with data and the analysis of prior work.

$$\beta/\Omega = aR \qquad Re \leq 1.5 \times 10^5 \tag{30a}$$

$$\beta/\Omega = 97.47\, R^{0.116} \qquad 1.5 \times 10^5 \leq Re \leq 3.0 \times 10^5 \tag{30b}$$

$$\beta/\Omega = 8.55 \times 10^{-3}\, R^{1.6} \qquad Re \geq 3.0 \times 10^5 \tag{30c}$$

The Reynolds number limits were chosen in view of the data presented by Law, Pierini, and Newman.[4]

The time-averaged convective diffusion equation for turbulent flow is the governing relation

$$9X\zeta \frac{\partial \theta}{\partial X} = 3\zeta^2 \frac{\partial \theta}{\partial \zeta} + \frac{\partial}{\partial \zeta} \left[\left(1 + \frac{X\zeta^3 f(R)}{R^{3/2}} \right) \frac{\partial \theta}{\partial \zeta} \right] \quad , \tag{31}$$

with boundary conditions

$$\theta = 1 \qquad \zeta = \infty \tag{32a}$$

$$\theta = 0 \qquad \zeta = 0 \qquad X \geq 0 \tag{32b}$$

$$\theta = 1 \qquad \zeta = 0 \qquad X < 0 \tag{32c}$$

where

$$X = 9K \int_{R_i}^{R} R\sqrt{R\ \beta/\Omega}\ dR \tag{33}$$

The function f(R) is defined by the following

$$f(R) = 0 \qquad R \leq 2.0 \times 10^5 \tag{34a}$$

$$f(R) = \frac{R - \sqrt{2.0 \times 10^5}}{\sqrt{3.0\times10^5} - \sqrt{2.0\times10^5}} \qquad 2.0 \times 10^5 \leqq Re \leqq 3.0 \times 10^5 \tag{34b}$$

$$f(R) = 1 \qquad Re \geqq 2.0 \times 10^5 \tag{34c}$$

The importance of the eddy diffusivity is reflected in the change of f(R) from 0 in the laminar region to 1 in the fully-developed turbulent flow region.

To obtain the concentration at the surface in addition to the current density distribution, the expression for the concentration derivative at the surface is the most useful form of the integral equation

$$\left.\frac{\partial c_i}{\partial y}\right|_{y=0} = -\left(\frac{\Omega^{1/2}K^{1/3}}{\nu^{1/6}D_i^{1/3}}\right)\sqrt{R\ \beta/\Omega}\int_0^z \left.\frac{dc_i}{dz}\right|_{z=z'} \frac{\theta_\zeta(z,z',\zeta=0)dz'}{(z-z')^{1/3}} . \tag{35}$$

$\theta_\zeta(z,z',\zeta=0)$ represents $\left.\frac{\partial\theta}{\partial\zeta}\right|_{\zeta=0}$ evaluated at position z for a step change in concentration that occurs at position z'. One should also note that the integral is a Stieltjes integral.

Solution Technique

Equation 35 governs the mass-transfer rate and equation 24 governs the potential distribution. As in earlier work[9,10], one alternates between revising the concentration distribution obtained from the mass-transfer equation and the potential distribution.

The integral equation is divided evenly in r^3. For each mesh point in r^3, a corresponding value of z exists defined by equation 27. If laminar

flow prevailed across the surface, the integral equation could be discretized in an efficient manner described by Acrivos and Chambré. However, since the flow regime varies, it is necessary to evaluate the following integral between adjacent mesh points.

$$\int_{z_i}^{z_{i+1}} \frac{\theta'(z_i,z',\zeta=0)}{(z-z')^{1/3}}\,dz' \tag{36}$$

By considering the logarithm of the integrand to be linear in log R, an analytic form is

$$\ln\left[\frac{z-z_{i+1}}{z-z_i}\right]\left\{\frac{\theta'(z,z_{i+1},\zeta=0)(z-z_{i+1})^{2/3}-\theta'(z,z_{i-1},\zeta=0)(z-z_i)^{2/3}}{\ln\left[\frac{\theta'(z,z_{i+1},\zeta=0)(z-z_{i+1})^{2/3}}{\theta'(z,z_{i-1},\zeta=0)(z-z_i)^{2/3}}\right]}\right\} \tag{37}$$

The discretized form is similar to the form of Acrivos and Chambré except that the constants are evaluated according to equation 37.

Results and Discussion

The results of the calculations are compared to the experiments of LaQue in figure 2. The physical properties and parameters used for the analysis are given in table II. It is interesting to note that the values shown in table II are reasonable values; no attempt was made to obtain a good fit by varying the program parameters. The calculations are qualitatively and quantitatively similar to LaQue's results.

For a 2.5 in. (6.35 cm) diameter disk, the current density and potential variations are presented in figure 3. Corrosion occurs over most of the disk, as the point of passivation is calculated to be $r_p/r_0 = 0.86$. The iron current density (corrosion rate) is substantially above the oxygen current density in the central region to compensate for the higher oxygen transfer rate

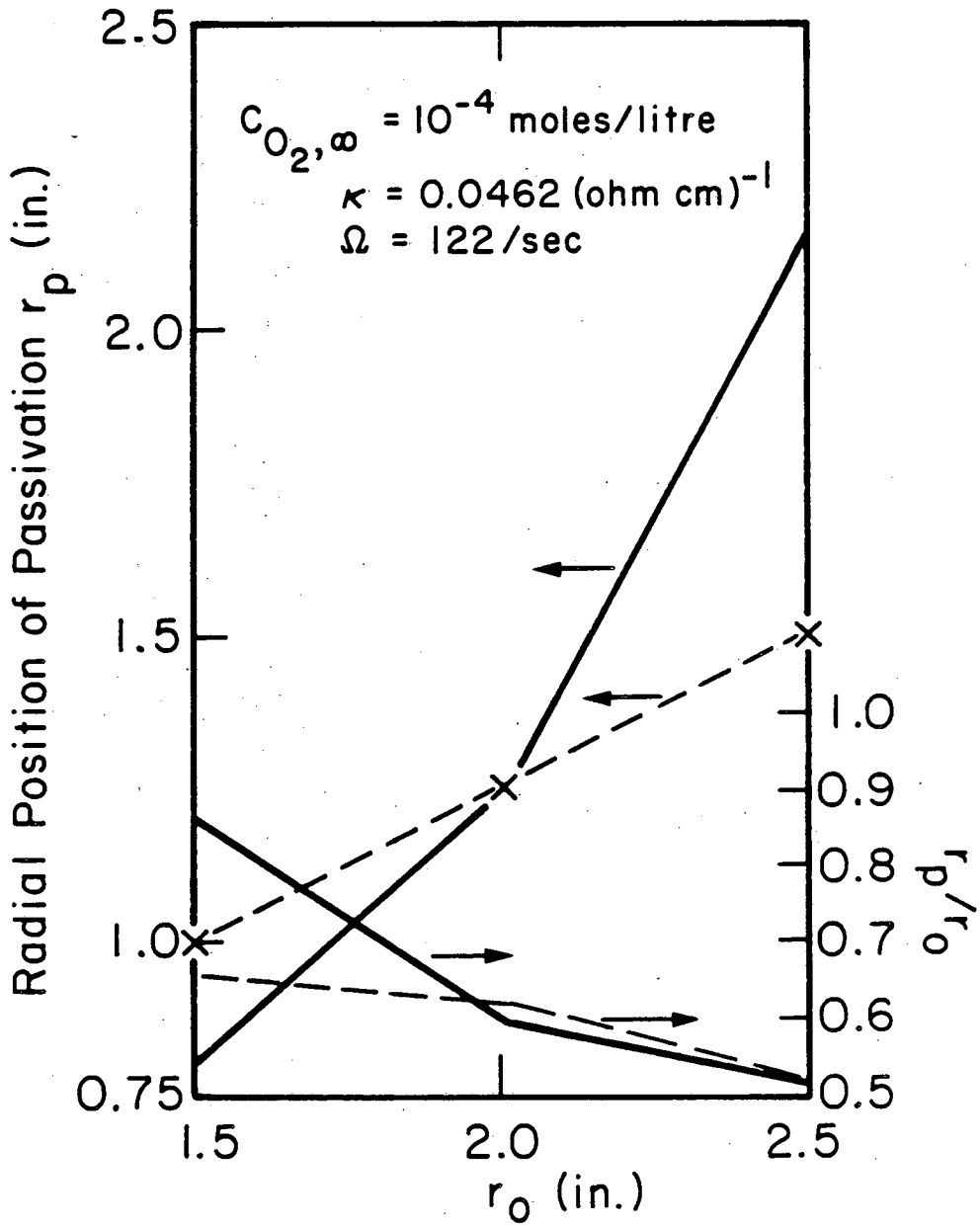

XBL 809-11886

Fig. 2 Comparison of the measured (---) and calculated (——) points of passivation for disks of different sizes.

near the edge. The oxygen current density is mass-transfer controlled. Hence the rate is uniform in the central region where laminar flow prevails. As shown previously, the mass-transfer rate decreases at the beginning of the transition region. Following the sharp dip, the mass-transfer rate increases for the remainder of the transition region. In the fully developed turbulent flow regime, the oxygen current density increases but more slowly than in the transition region.

The variation of the ohmic potential is provided in figure 3 for reference. Φ_o is more positive in the center of the disk than near the edge. This is a consequence of the higher anodic current density in the center and higher cathodic current density near the edge.

Table II

Additional Parameters

D_{O_2}	=	$1.3 \times 10^{-5} cm^2/s$
D_{OH^-}	=	$5.26 \times 10^{-5} cm^2/s$
$D_{Fe^{++}}$	=	$0.739 \times 10^{-5} cm^2/s$
c_{OH^-}	=	$1.0 \times 10^{-7} mol/\ell$
$c_{Fe^{++}, \infty}$	=	0
κ_∞	=	$0.0462\ (ohm\text{-}cm)^{-1}$ [12]

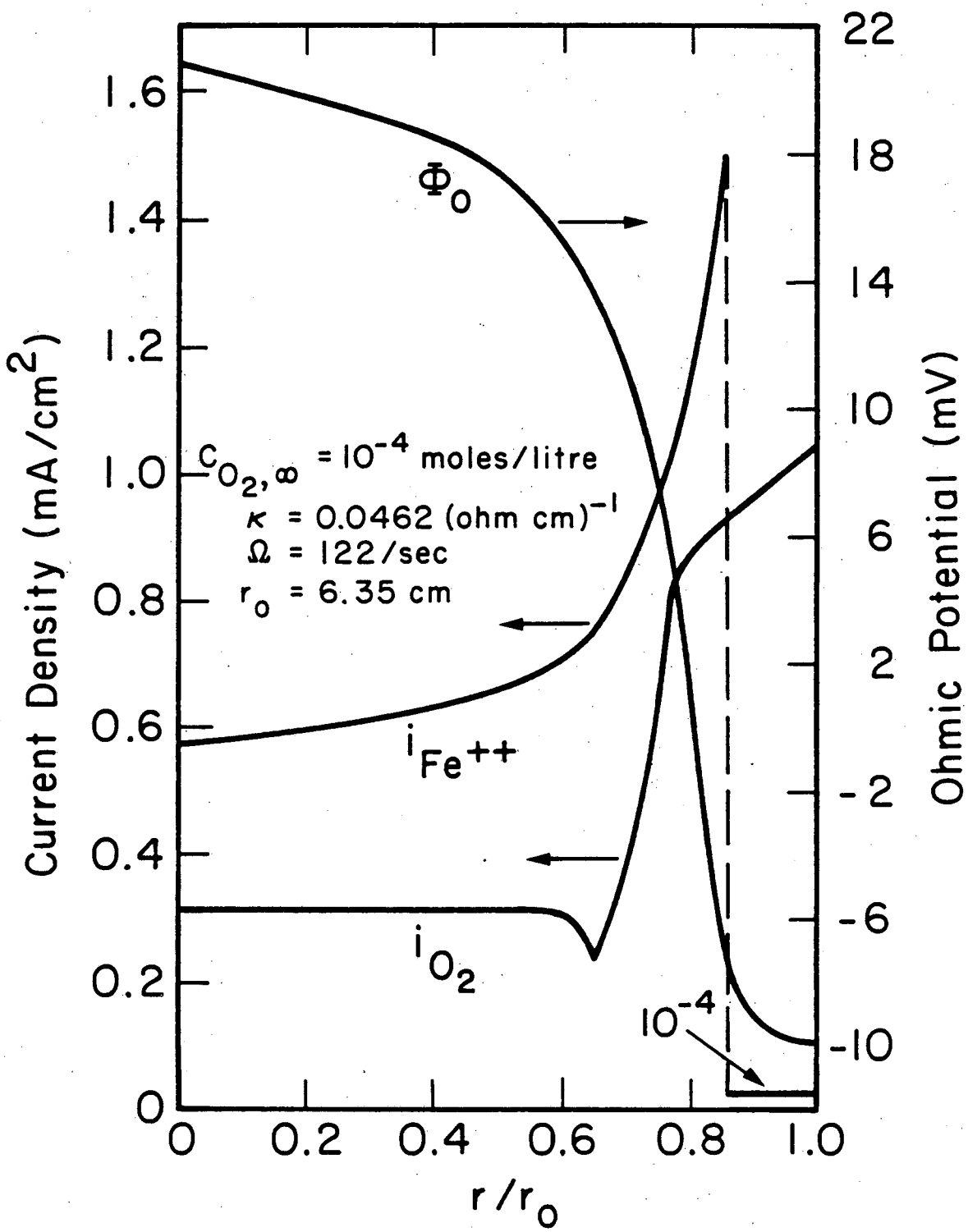

XBL 809-11884

Fig. 3 Current and potential distributions.

The surface concentrations corresponding to the curves in figure 3 are presented in figure 4. Since oxygen is at the limiting current, its concentration is zero across the surface. The surface concentrations of the ferrous and hydroxyl ion do not have any significant impact upon the results. This becomes apparent from an observation of the kinetic expressions in which they appear. The ferrous ion is a factor in the cathodic term of the oxidation reaction, and the hydroxyl ion is in the anodic term of the reduction reaction. Both these terms make an insignificant contribution to their respective reactions. For different values of the bulk pH, this may not be true. Consequently, the OH^- concentration is determined from the flux of oxygen. The sharp change in the iron concentration illustrates the change from the active to the passive state.

Results are presented in figure 5 which illustrate the effect of the oxygen concentration on the corrosion level and its distribution. The oxygen concentration is half the value used in figure 3. All other parameters are the same. For the lower concentration and lower mass-transfer rate, the point of passivation moves inward, since the total iron rate must be equivalent to a decreased oxygen rate. Although corrosion takes place over a smaller portion of the disk, the average corrosion rate is higher on the active portion with the lower oxygen concentration.

Results illustrating the effect of solution conductivity are presented in figure 6. One expects the corrosion rate to be higher for the higher conductivity, since the ohmic drop will be lower. In addition, the corrosion occurs over a smaller portion of the disk to balance the unchanged oxygen transfer rate.

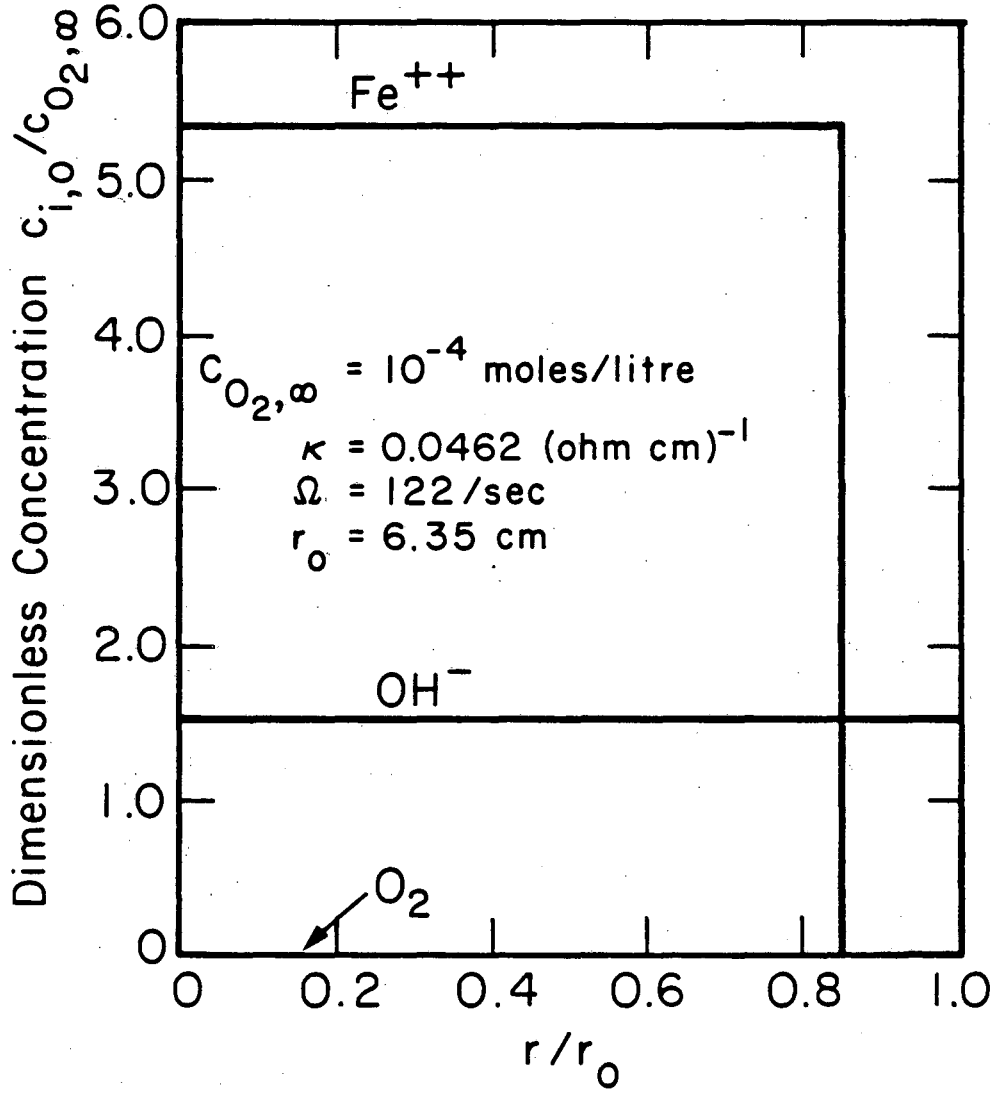

XBL 809-11883

Fig. 4 Dimensionless concentration distribution.

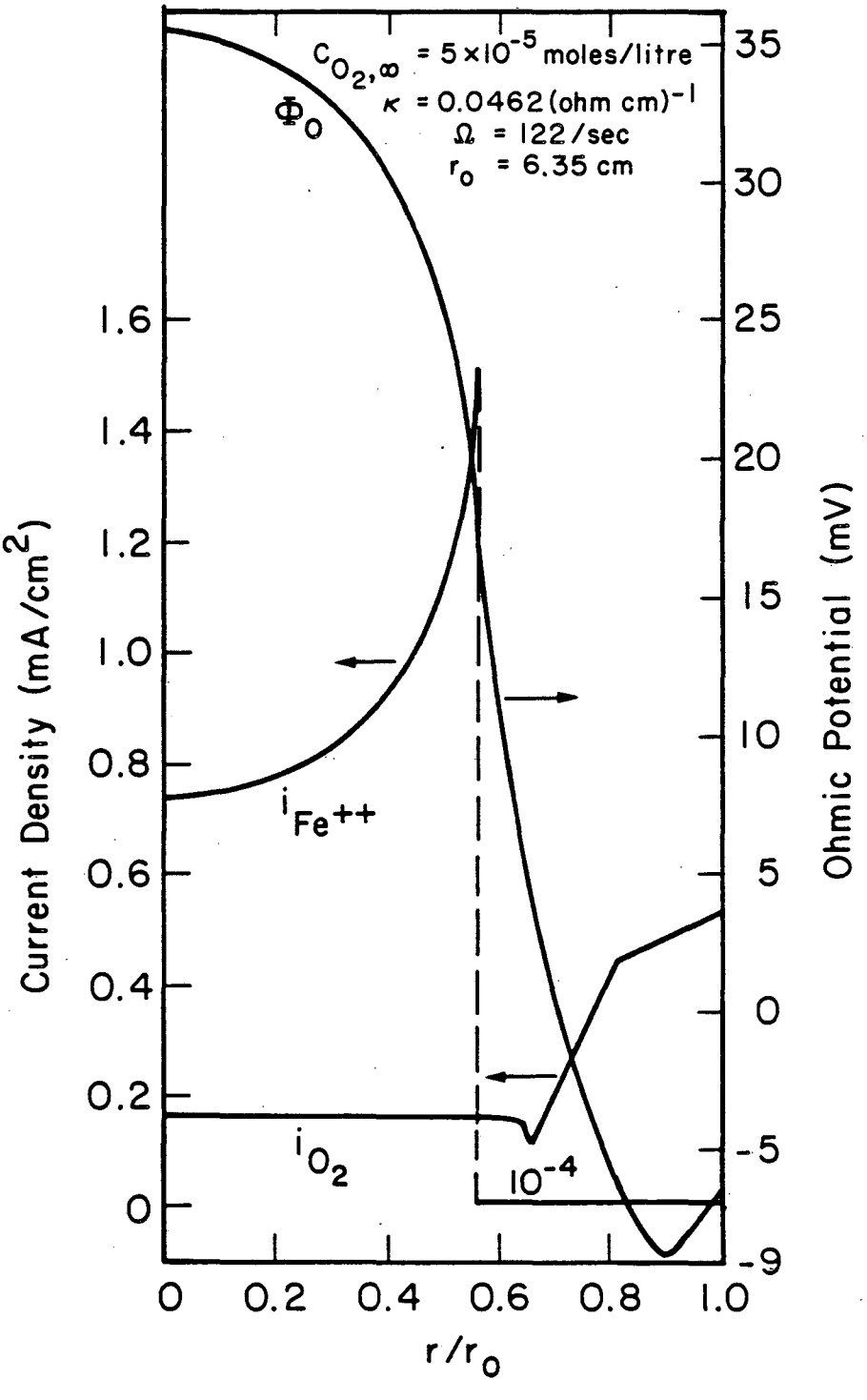

XBL 809-11885

Fig. 5 Current and potential distributions.

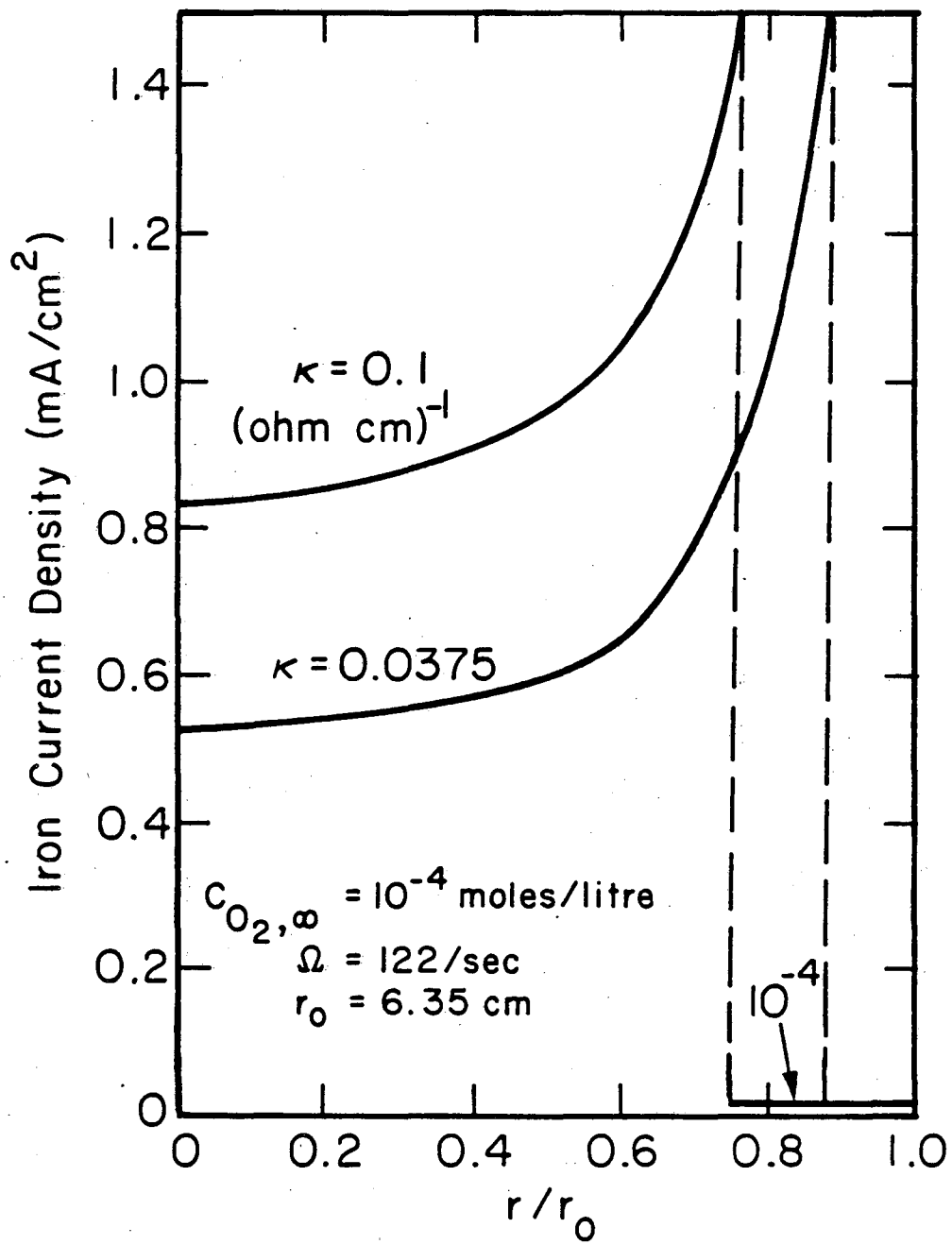

XBL 809-11887

Fig. 6 The effect of conductivity on the corrosion rate distribution.

It is also interesting to note that for conductivity values lower than about 0.035 $(ohm\text{-}cm)^{-1}$ corrosion will not occur (using the parameters previously defined). The conductivity is so low and the ohmic drop so severe that the iron reaction can not balance the oxygen transfer. Hence the potential is shifted to values such that the entire surface is passivated.

An envelope is presented in figure 7 which separates the corrosion region from the passive domain. Above the line, the disk is completely passive, whereas below the line portions of the disk may be active and passive. The axes are approached assymptotically. The rotation speed reflects changes in the oxygen transfer rate, whereas the mass-transfer rate and ohmic considerations are affected by the radius.

Summary and Conclusions

Results are presented for a model which considers the electrochemical corrosion of an iron disk. The hydrodynamics vary from laminar flow in the center to fully-developed turbulent flow at the periphery. The active-passive nature of iron is considered very sharp. Good agreement is obtained between the results of this model and the experimental observations reported by LaQue. The importance of conductivity, oxygen concentration, and disk size on the overall results is illustrated.

Acknowledgment

This work was supported by the United States Department of Energy under Contract No. DE-AC03-76SF00098 through the Director, Office of Energy Research, Office of Basic Energy Sciences, Chemical Sciences Division, and through the Assistant Secretary of Conservation and Renewable Energy, Office of Advanced Conservation Technology, Electrochemical Systems Research Division.

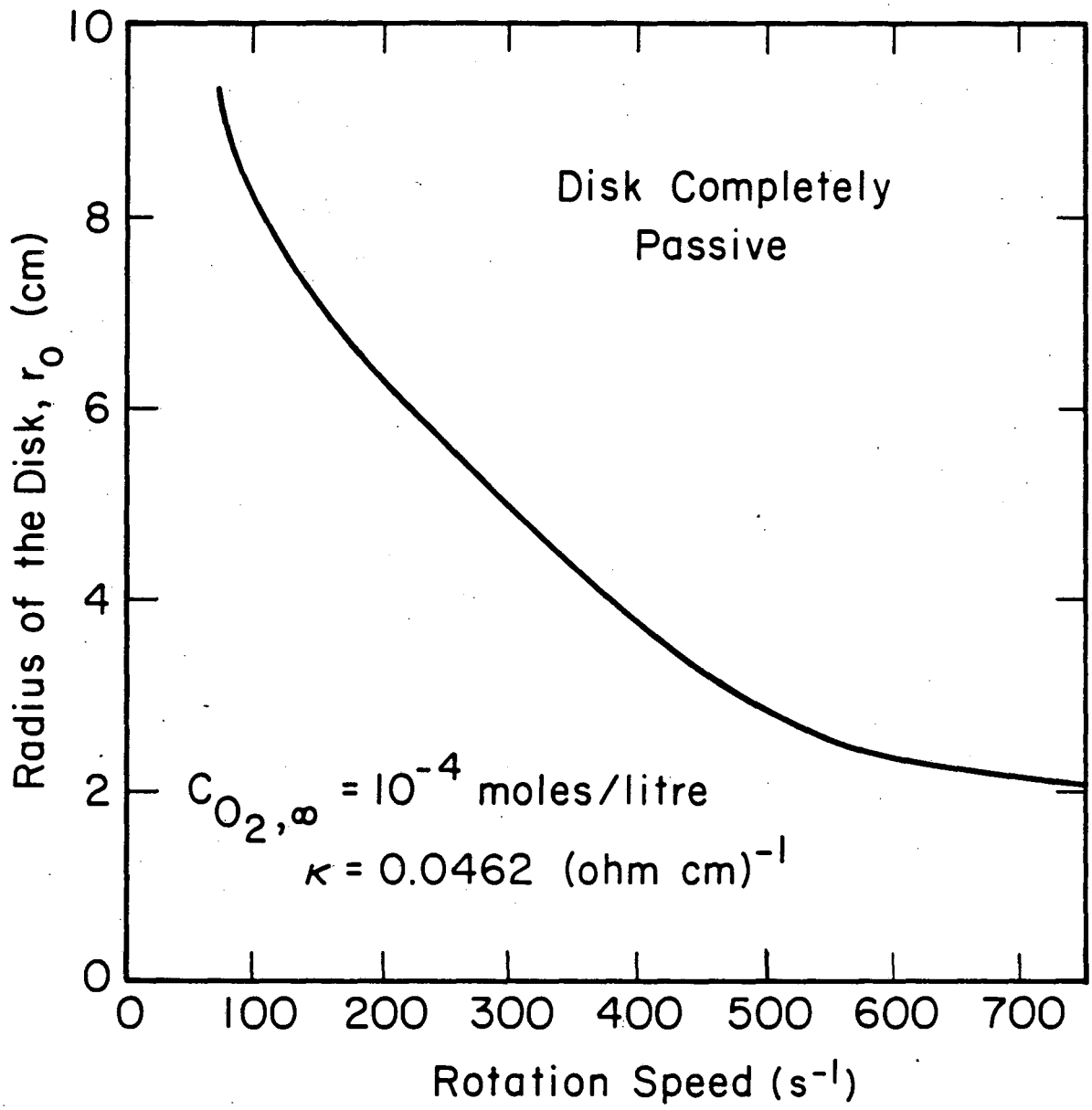

Fig. 7 Envelope indicating region of passivity.

Nomenclature

a	0.51023262
B_n	coefficient in the expansion for the potential
$c_{Fe^{++},0}$	concentration of ferrous ions at the disk surface, mole/litre
$c_{OH^-,0}$	concentration of hydroxyl ions at the disk surface, mole/litre
c_i	concentration of species i, mole/litre
$c_{i,0}$	concentration of species i at the surface, mole/litre
$c_{i,\infty}$	bulk concentration of species i, mole/litre
D_i	diffusion coefficient of species i in the electrolyte, cm^2/s
F	Faraday's constant, 96487 C/mole
$f(R)$	function defined in equation 34
i_j	local current density of reaction j, A/cm^2
i_p	current density on the passive portion of the disk, A/cm^2
$i_{0,j}$	exchange current density for reaction j, A/cm^2
$i_{0j,ref}$	reference exchange current density for reaction j, A/cm^2
i_T	total current density, A/cm^2
I	total current on the disk, A
$I_{Fe^{++}}$	total current from the iron reaction, A
I_{O_2}	total current from the oxygen reaction, A
K	constant for the eddy diffusivity, 2.9×10^{-3}
M_i	symbol for the chemical formula of species i
M_{2n}	Legendre function of imaginary argument
n_j	number of electrons transferred in reaction j
N_i	flux of species i, $mole/cm^2\text{-}s$
P_{2n}	Legendre polynomial of order 2n

q_{ij}	reaction order for cathodic reactants
Q_n	coefficient in the expansion for the potential, V
r	radial coordinate, cm
r_o	disk radius, cm
r_p	radius of the active portion of the disk, cm
R	universal gas constant (8.3143 J/mol — K)
R	dimensionless radius
Re	Reynolds number
s_{iref}	stoichiometric coefficient of species i in reference electrode reaction
s_{ij}	stoichiometric coefficient of species i in reaction j
T	absolute temperature, K
U_j^θ	standard electrode potential for reaction j, V
$U_{j,o}$	theoretical open circuit potential for electrode reaction j of the composition prevailing locally at the disk surface relative to a reference electrode of a given kind, V
U_{ref}^θ	standard electrode potential for reference reaction, V
V_M	defined by equation 14, V
V	disk potential, V
$(V-\Phi_o)_*$	passivation potential, V
x	distance in direction of flow
X	dimensionless variable defined in equation 33
y	axial coordinate, cm
z_i	charge of species i
z	dimensionless stretched radial coordinate

Greek Letters

α_a	anodic transfer coefficient
α_c	cathodic transfer coefficient
β	proportionality of v with y, s
γ_{ij}	exponent in equation 8
η	rotational elliptic coordinate
η_s	local surface overpotential, V
κ_∞	bulk solution conductivity, $(\text{ohm-cm})^{-1}$
θ	dimensionless concentration
ν	kinetic viscosity, cm^2/s
ρ_o	density of pure solvent, g/cm^3
ξ	rotational elliptic coordinate
Φ_o	electric potential in the solution immediately adjacent to the disk surface, V
ζ	Lighthill variable
Ω	rotation speed of the disk, s^{-1}

References

1. J. Newman, "Mass Transport and Potential Distribution in the Geometries of Localized Corrosion," presented before National Association of Corrosion Engineers, December, 1971, Williamsburg, Virginia.

2. J. Newman, "Current Distribution on a Rotating Disk below the Limiting Current," Journal of the Electrochemical Society, 113, 1235-1241 (1966).

3. V. G. Levich, "The Theory of Concentration Polarization," Acta Physiochimica URSS, 17, 257-307 (1942).

4. C. G. Law, Jr., P. Pierini, and J. Newman, "Mass Transfer to Rotating Disks and Rotating Rings in Laminar, Transition, and Fully-Developed Turbulent Flow," International Journal of Heat and Mass Transfer, 24, 909-918 (1981).

5. F. L. LaQue, "Theoretical Studies and Laboratory Techniques in Sea Water Corrosion Testing Evaluation," Corrosion, 13, 303t-314t (1957).

6. N. Vahdat and J. Newman, "Corrosion of an Iron Rotating Disk," Journal of the Electrochemical Society, 120, 1682-1686 (1973).

7. M. Pourbaix, "Some Applications of Electrochemical Thermodynamics," Corrosion, 6, 395-404 (1950).

8. W. H. Smyrl and J. Newman, "Ring-Disk and Sectioned Disk Electrodes," Journal of the Electrochemical Society, 119, 212-219 (1972).

9. W. R. Parrish and J. Newman, "Current Distribution on a Plane Electrode Below the Limiting Current," Journal of the Electrochemical Society, 116, 169-172 (1969).

10. R. White and J. Newman, "Simultaneous Reactions on a Rotating Disk Electrode," Journal of Electroanalytical Chemistry and Interfacial Electrochemistry, 82, 173-186 (1977).

11. A. Acrivos and P. L. Chambré, "Laminar Boundary Layer Flows with Surface Reactions," Industrial and Engineering Chemistry, 49, 1025-1029 (1957).

12. R. C. Weast and M. J. Astle, editors, Handbook of Chemistry and Physics, sixty-third edition, (Boca Raton, Florida: Chemical Rubber Company Press, Inc., 1982), page D-258.

This report was done with support from the Department of Energy. Any conclusions or opinions expressed in this report represent solely those of the author(s) and not necessarily those of The Regents of the University of California, the Lawrence Berkeley Laboratory or the Department of Energy.

Reference to a company or product name does not imply approval or recommendation of the product by the University of California or the U.S. Department of Energy to the exclusion of others that may be suitable.

TECHNICAL INFORMATION DEPARTMENT
LAWRENCE BERKELEY LABORATORY
UNIVERSITY OF CALIFORNIA
BERKELEY, CALIFORNIA 94720